

# A Novel Estimation of Tearing Limit in Deep Drawing Process Based on Strain Energy; Experimental Characterization and Numerical Validation

Ahmad Aminzadeh (✉ [ahmad.aminzadeh@uqar.ca](mailto:ahmad.aminzadeh@uqar.ca))

University of Quebec in Rimouski: Universite du Quebec a Rimouski

Mohammad Khaboushani

University of Tehran

Ali Parvizi

University of Tehran

---

## Research Article

**Keywords:** Slab method, deep drawing process, blank holder force, tearing limit, strain energy

**Posted Date:** April 12th, 2022

**DOI:** <https://doi.org/10.21203/rs.3.rs-1520328/v1>

**License:**  This work is licensed under a Creative Commons Attribution 4.0 International License.

[Read Full License](#)

---

# **A Novel Estimation of Tearing Limit in Deep Drawing Process Based on Strain Energy; Experimental Characterization and Numerical Validation**

Mohammad Khaboushani<sup>1</sup>, Ahmad Aminzadeh<sup>\*2</sup>, Ali Parvizi<sup>1</sup>

*1- School of Mechanical Engineering, College of Engineering, University of Tehran, Tehran, Iran*

*2- Department of Mathematics, Computer Science and Engineering, Université du Québec à Rimouski,  
Rimouski, Québec, Canada*

*\*Corresponding author: ahmad.aminzadeh@uqar.ca*

## **Abstract**

Deep drawing is a forming process widely used in aerospace, military, automotive, and various industries. One of the essential useful parameters in the quality of deep-drawn products is Blank Holder Force (BHF). By Controlling BHF during the process, formability has been improved, reduced forming energy, and sheet thickness. Tearing is one of the most common and crucial defects in this process due to high radial stress in the cup's wall, resulting in many limitations in this field. In this process, the blank holder force plays an indispensable role in causing tearing. Therefore, controlling blank holder force during the process would be inevitable to avoid tearing or even wrinkling. This study aims to calculate the tearing limit with new criteria in analytical dominating plasticity Equations based on the slab Method. The St14 sheet with 1 mm thickness and 200 mm diameter is used in this study. The maximum blank holder force in each stage of punch stroke with new criteria based on strain energy with three different frictional coefficients is calculated, compared, and verified with FEM simulation and experimental results. Analytical results with new criteria are also compared with previous procedures. Finally, it is realized that results related to energy criteria have a lot more similarity with FEM simulation and experimental results in comparison with the previous ones.

**Keywords:** *Slab method, deep drawing process, blank holder force, tearing limit, strain energy.*

## 1. Introduction

A manufacturing company's mission today is to create high-quality products with no defects, reduce lead times, and increase production rates. Metal forming is an integral part of deformation-based manufacturing. These mechanical components can be found in automobiles [1], aerospace [2], home appliance industry [3], and food industry [4]. In addition to its strength and durability, metal manufacturing is also crucial for all sectors of the economy. It is possible to fabricate metal components in as many ways as desired, but deep drawing is the most common metal forming process used when a cup-like cylindrical component is to be made by radially drawing the metal blank into a die. With deep drawing, metals are reshaped while still solid by taking advantage of the plasticity of certain metals. In order to plastically deform a metal, more force must be applied than the yield strength. The deep drawing process, however, entails a number of problems including wrinkles, ruptures, tearing, and cracking. Several methods can be used to identify and detect the process parameters used during the forming process. Many key parameters are taken into account in deep drawing, including blank holder force, friction coefficient, die configuration, and material characterization. For assessing the effect of process parameters and determining the optimal process parameters in deep drawing, researchers have recently proposed online monitoring methods. Using deep drawing parameters, Dwivedi et al. [5] identified directions for future research, and the results of the present study demonstrated the production of aluminum alloy cups successfully. Numerous studies have been conducted on the experimental aspect of key process parameters and the impact they have on objective function [6–10].

As demonstrated by Padmanabhan et al. [11], Variables such as die radius, holder force, and friction coefficient affect the deep-drawing characteristics of axis-symmetric stainless steel cups more than other parameters. In addition to the blank holder force and the friction coefficient, the small die radius can also affect the blank holder force and the friction coefficient. Experimentally, Afshin et al. [12] shown in a deep-drawing process using laminated sheets, demonstrate the ability to thin and wrinkle materials such as Al 1050/St 304 and Al 5052/St 304. As a result of the study, their results indicate that the blank holder force (BHF) determines the forming load variation when the temperature is raised. Research by Reddy et al. [13] has investigated the effects of key process parameters (punch nose radius, die shoulder radius, and blank holder force). Consequently, the blank holder force (56.98%) was the most significant parameter, followed by punch nose radius (30.12%), and the die profile radius (12.90%) was the least significant parameter. The influence

of the aluminum alloy AA5754-O on the blank holder and sheet plate during the forming process was investigated by Demirci et al. [14] by applying variable forces in a computer-controlled manner to the blank holder and sheet plate. According to their findings, the best formation occurred at a pressure of 5 MPa. In [15], numerical analysis and experimental validation of deep drawing were performed for the purpose of preventing thinning and wrinkles. Deep-drawn cups commonly tear due to a crack near the bottom of the vertical wall caused by high tensile stress that results in thinned and cracked metal. Two analytical approaches are proposed to predict the safe area in the forming operation: slab [16] and upper bound [17]. Friction is considered in the Slab Method (SM), also called Stress Local Analysis Method (SLA). Consequently, the results obtained by employing this method are generally better than the ones obtained by using other methods. Rubio [18] evaluated tube drawing processes by an analytical model employing the slab method (SM) and the upper bound method (UBM). The plastic deformation zone is also modeled using Triangular Rigid Zones (TRZ). In order to understand the wrinkling limit diagram for two-layer sheets, Bagdad et al. [19] used a mathematical model, a numerical method, and experimental tests. The authors conclude that materials properties, blank geometry, and stack order influence optimum blank holder forces. During deep drawing of two-layer (aluminum-stainless steel) sheets, we developed an analytical method, performed numerical simulations, and performed experiments to investigate the effects of wrinkling. Our results show that the optimum BHF is affected by the geometry of the sheet, the properties of the material, and the layup. The study by Gharib et al. [21] proposes an optimization method for linearly varying blank holder force (BHF) that seeks to minimize the maximum punch force and avoid process limitations. In their study, they found that the slope of the linear BHF increases linearly with drawing ratio. Additionally, the intercept of the function showed a nearly linear relationship to the drawing ratio. Following is an equation that shows what force is optimal regardless of drawing ratio. Because metal parts are nonlinearly deformed, there are many different types of stress distributions. Large deformations can cause meshes to distort and generate defects [22]. For this reason, selecting the right formulation for developing an appropriate FE model for the problem is crucial. Sugiyanto et al. [23] developed a finite element model based on the Finite Element Method (FEM) to evaluate the effect of a blank holder on the deep drawing process. The clearance variable should result in a decrease in the force required for deep drawing, according to simulations of this process without blank holders. Nevertheless, the force required for the drawing will still be greater. A 3-D finite element simulation was used to

analyze the hydro-mechanical deep drawing process of anisotropic laminated bimetallic sheets with an implementation of a Fortran-based code to accurately model the distribution of non-uniform oil pressure in Bagherzadeh et al. [24]. As part of their study of force control in deep drawing, Yoshihara et al. [25] used finite element simulations to verify the LDR of magnesium alloy sheets. In FEM simulations, we confirm that the behavior resembles that observed in experiments, with rupture occurring during the fracture at the wall. Sheng et al. [26] developed an adaptive simulation strategy during the simulation process. By doing so, it is possible to predict a BHF profile from a single simulation, thereby reducing computation time. The proposed strategy has been successfully applied to several conical cup drawing operations. To compare the predictions, experimental results have been used, and they show that the adaptive simulation strategy may also be useful for improving drawing for non-symmetric parts. Qin et al. [27] have developed a blank holding technique that allows blank holding force (BHF) to be independently loaded during sheet metal forming using electro-permanent magnets (EPM). The theoretical method and FEM are used to analyze and solve the coupling problem involving the magnetic field and stress field. Also, the new technique can be used to obtain the blank holding force and the BHF on the sheet. Despite the design cushion's BHF being large enough, the selected sheet could go through a deep drawing process with the BHF applied through the design cushion.

To the best of the authors' knowledge, there is a lack of investigating the numerical solution, FEM simulation, and experimental of the deep drawing process for estimate tearing limit with slab method and new criteria based on strain energy. In order to prevent cracking, this study provides a suitable mathematical approach to determine the maximum BHF over the punch stroke. Furthermore, a new method based on strain energy was used to predict the tearing limit. The SLAB method's methodological perspective to assuming a constant volume of material was used to evaluate stress and strain in the deep-drawn cup. The impact of friction and material anisotropy were also taken into account in the study. In order to assure the accuracy of analytical results, an adequate number of experiments as well as FEM simulations were carried out, and the results of these two parts were verified with each other. It is also important to note that previous methods estimated the tearing limit, and the results of these two methods were compared with experimental and FEM ones. The following scheme diagram shows the concept of this study as a systematic investigation (Figure 1). As can be seen in Fig.1, firstly, FEM simulation was carried out precisely, and then they were verified with experimental ones. At the next stage, FEM simulations were done

with various BHF's as the inputs, and drawn depths at the tearing moment were measured in ABAQUS. At the next stage, contrary to the previous stage, the  $h_i(s)$  calculated from ABAQUS were considered as the input in analytical calculations, and corresponding to each  $h_i$ , its BHF was calculated as the output. Furthermore, a group of  $h_i(s)$  and BHF(s) were achieved with two different methods (FEM and new analytical approach), and finally, they were compared to each other. They were also compared with previous analytical methods to evaluate the practicality of the new criteria to estimate BHF during the deep drawing process.

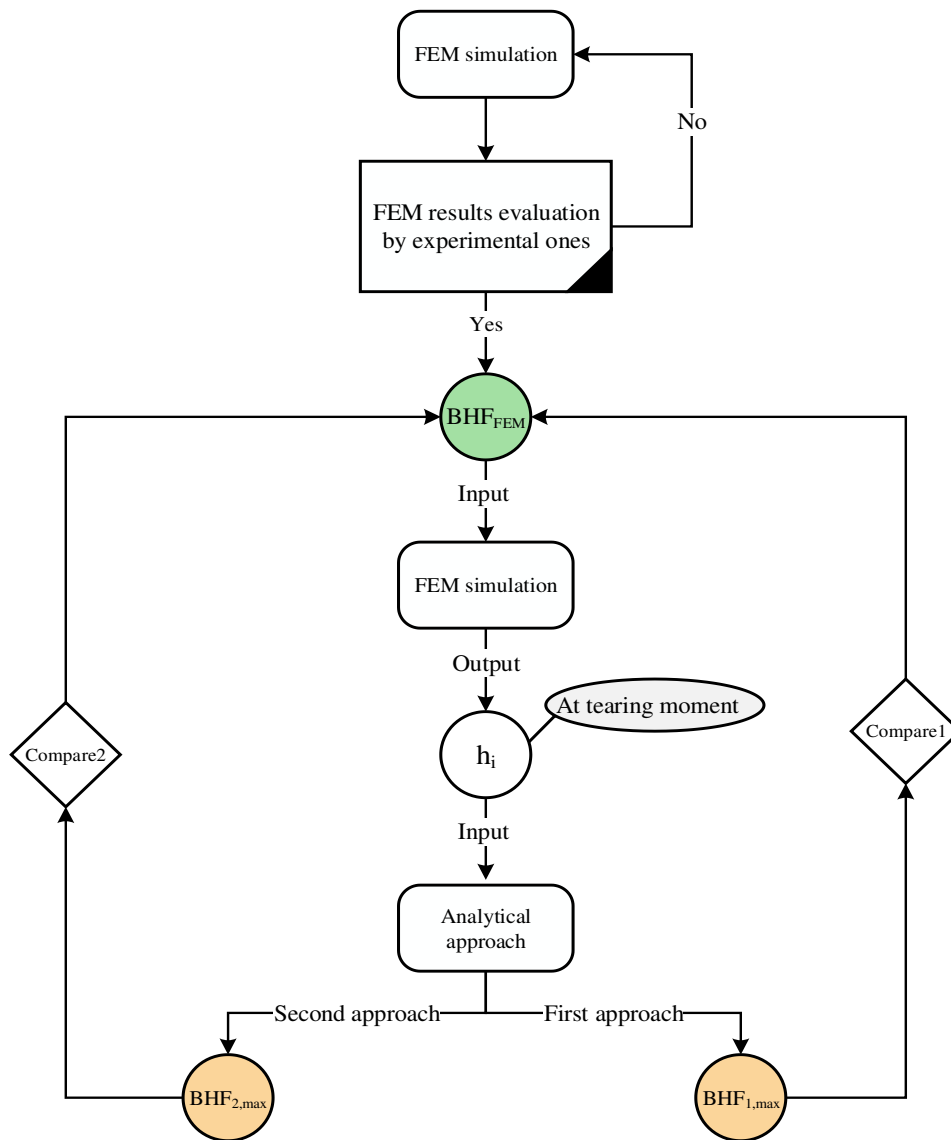


**Fig.1.** Flow chart of the validation and calculation of  $BHF_{max}$ .

## 2. Analytical method

## 2.1.Radial stress calculation in the flange

In this section, the slab method was used to anticipate the maximum blank holder force along the punch stroke with the following assumptions:

1. The volume of the sheet during the process is considered constant.
2. The Tresca yield criterion is used to calculate the Equilibrium stress.
3. The metal flow in the flange part is considered a plane strain.
4. The effects of friction and material anisotropic are also considered in the analysis.

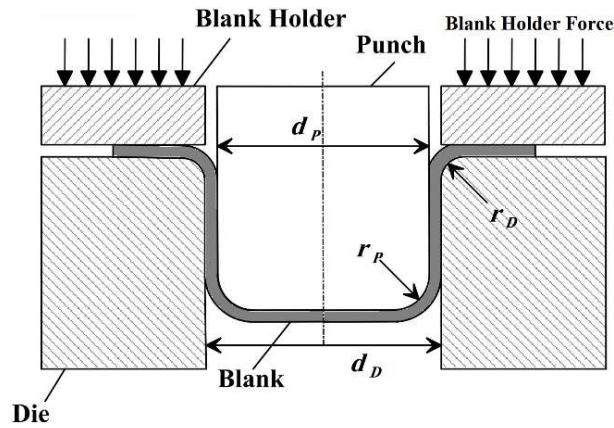
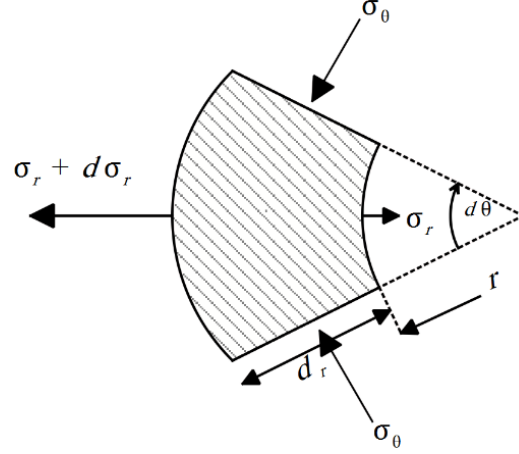


Fig. 2. Deep drawing process

Axial and radial stresses in an element can be seen from Fig. 3. Under the condition of force equilibrium in a an element of the flange and the absence of friction, the radial stress mathematical equation can be obtained as follows:

$$rd\sigma_r d\theta t_0 - \sigma_r d_r d\theta t_0 - 2\sigma_\theta \sin \frac{d\theta}{2} dr t_0 = 0 \quad (1)$$



**Fig. 3.** The Equilibrium force diagrams of the flange in a small element

Where  $r$  is the inside radius,  $\sigma_r$  is the radial stress,  $d\theta$  is a small portion angle of the flange,  $t_0$  is the initial thickness of the sheet, and  $\sigma_\theta$  is the tangential stress in the flange. As  $d\theta/2$  is very small, it can be considered to be equal to  $\sin(d\theta/2)$ . Therefore, by simplifying Eq(1), the following relation is obtained:

$$d\sigma_r = (\sigma_r - \sigma_\theta) \frac{dr}{r} \quad (2)$$

Considering Tresca criteria:

$$\sigma_r - \sigma_\theta = \sigma_f \quad (3)$$

By substituting Eq (3) into Eq (2) and integrating Eq (2), the radial stress is obtained at each stroke of the forming process, as follows:

$$\sigma_{r,i} = \sigma_f \ln \frac{R_{1,i}}{r_i} \quad \text{Or} \quad \sigma_{r,i} = \sigma_f \ln \frac{d_{1,i}}{d_i} \quad (4)$$

Where,  $\sigma_f$  is the mean flow stress between points 1 and 2, flange segment, in Fig.4.,  $d_{1,i}$  is the outer diameter of the flange in each step of the process, and  $d_i$  is the average diameter of the cylindrical cup or the inner die diameter minus the sheet thickness.

## 2.2.The effect of sheet anisotropy on radial stress

As can be seen from Eq (4), radial stress can be calculated, regardless of the anisotropy coefficients. In order to simplify the effect arising from sheet anisotropy on radial stress, Hill's relation for a planar isotropy material was used in this regard; using this, the following relation is established:

$$(\sigma_r - \sigma_z)^2 + (\sigma_\theta - \sigma_z)^2 + R(\sigma_r - \sigma_\theta)^2 = (R + 1)X^2 \quad (5)$$

As sheet deviation in thickness, just in flange area because of small deviation in this area, can be ignored, so:

$$d\varepsilon_z = d\lambda[F(\sigma_z - \sigma_\theta) - G(\sigma_z - \sigma_r)] = 0 \quad (6)$$

Since, in a Planar isotropy condition,  $F = G$ , so:

$$\sigma_z = \frac{\sigma_r + \sigma_\theta}{2} \quad (7)$$

By substituting Eq (7) into Eq (5), in case that the equivalent stress is Equal to the flow stress, so:

$$\sigma_r - \sigma_\theta = \sqrt{\frac{2(R + 1)}{2R + 1}} \sigma_f \quad (8)$$

### 2.3. Calculation of radial stress of the wall in 3 parts of the cup by strain relief

This section aims to estimate the radial stress in different parts of the cup along the punch stroke. As shown by Fig. 3, to calculate radial stress in different parts of the sheet, in this method, the sheet is divided into two parts. Calculating strain at different stages of the process is necessary to calculate stress in the wall during the forming process. With strain at points 1, 2, and 3 of the sheet and plastic properties of the sheet along the punch stroke, it is possible to calculate flow stress in different sheet parts using work hardening relations. For this purpose, it is first essential to calculate the outer diameter of the sheet at different deep drawing stages. Considering that the volume of the sheet is assumed constant before and after the process, by writing the Equilibrium volume Equation for a cylindrical cup with bends as is illustrated by Fig. 2, the outer diameter along punch stroke is obtained as follows: [29]

$$d_{1,i} = \sqrt{d_0^2 - 4d_D[h_i - (0.43r_p - 0.43r_D)]} \quad (9)$$

Where  $h_i$  is the height of the cup or punch displacement,  $d_D$  is the internal diameter of the die,  $r_D$  is die edge radius,  $d_0$  is the initial outer diameter of the sheet and  $d_{1,i}$  is the outer diameter along punch stroke. As shown by Fig. 4 and with  $d_{1,i}$  and  $d_0$ , it is possible to calculate the Equivalent strain at point 1 at different punch movement stages, according to Eq(12).

In order to calculate the Equivalent strain at point 2, it is necessary to calculate the length of this point (twice the distance from point 2 to the z-axis, Fig. 4.) at different stages of the deep drawing process. Given that the material volume at the initial outer diameter  $d_0$  to the initial stage of the sheet at point 2 ( $d_{int.i}$ ) is always constant by writing the Equilibrium of volume in this distance

and at different stages of the punch movement, the mathematical Equation of  $d_{int,i}$  can be written as follow;

$$t_0 \left( \frac{\pi d_0^2}{4} - \frac{\pi d_{int,i}^2}{4} \right) = t_0 \left( \frac{\pi d_{1,i}^2}{4} - \frac{\pi (d_D + 2r_D)^2}{4} \right) \quad (10)$$

By simplifying Eq (10) and having  $d_{1,i}$  at each step of the punch stroke and as the other parameters are constant,  $d_{int,i}$  can be calculated at each step of the punch stroke as follows.

$$d_{int,i} = \sqrt{d_0^2 + (d_D + 2r_D)^2 - d_{1,i}^2} \quad (11)$$

It is important to note that both of  $d_{1,i}$  and  $d_{int,i}$  are functions of the height of the cup or the punch stroke ( $h_i$ ).

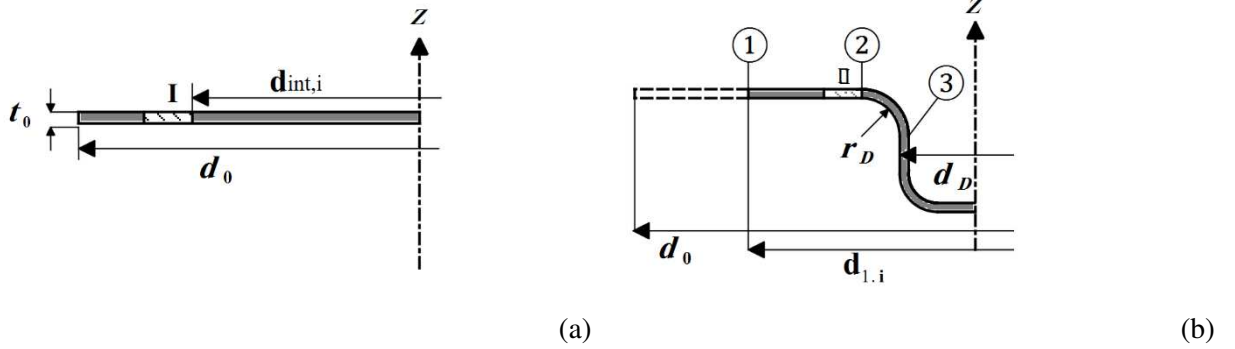


**Fig. 4.** Different steps of deep drawing process (a) first step (b) second step

Therefore, by computing  $d_{1,i}$  and  $d_{int,i}$  and taking into account the anisotropy of the sheet in calculations. The Equivalent strain at points 1 and 2 can be obtained at each step of the punch stroke following Eq (12) and (13):

$$\varepsilon_{1,i} = \sqrt{\frac{2(R+1)}{2R+1}} \ln \frac{d_0}{d_{1,i}} \quad (12)$$

$$\varepsilon_{2,i} = \sqrt{\frac{2(R+1)}{2R+1}} \ln \frac{d_{int,i}}{d_D + 2r_D} \quad (13)$$

After calculating the Equivalent strains, the mean flow stress between points 1 and 2 can be calculated according to Eq (14) and (15):

$$\sigma_{f1-2,i} = \frac{1}{2} k (\varepsilon_{1,i}^n + \varepsilon_{2,i}^n) \quad (14)$$

$$\sigma_{f1-2,i} = \frac{1}{2}k(\varepsilon_{1,i}^n + \varepsilon_{2,i}^n) + \sigma_0 \quad (15)$$

Where  $k$  is the strength coefficient of the material,  $n$  is the strain hardening exponential of material. Depending on the type of work hardening relation, both Eq (14) and (15) can be used. In this research, it is worth mentioning that tensile tests were conducted, and the interpolation of stress and strain data were conducted by MATLAB software. According to the MATLAB software's estimated function, Eq (15) is used to estimate the work-hardening relation. Besides, taking into account the bending effects in this region, the Equivalent strain at point 3 was calculated as following [29]:

$$\varepsilon_{3,i} = \varepsilon_{2,i} + \sqrt{\frac{2(R+1)}{2R+1}} \ln\left(1 + \frac{t_0}{2r_d + t_0}\right) \quad (16)$$

According to the sheet deformation, when it flows over the die radius and under bending condition, mean flow stress can be anticipated either by Eq (17) or (18):

$$\sigma_{f2-3,i} = \frac{1}{2}k(\varepsilon_{2,i}^n + \varepsilon_{3,i}^n) \quad (17)$$

$$\sigma_{f2-3,i} = \frac{1}{2}k(\varepsilon_{2,i}^n + \varepsilon_{3,i}^n) + \sigma_0 \quad (18)$$

As the estimated function, arising from tensile test data in the plastic region, had more conformity with Eq (18), it is used as work-hardening relation. MATLAB is used for regression in which  $k$ ,  $n$ , and  $\sigma_0$  are calculated 359.3, 0.7718, and 223.3 respectively.

#### 2.4. Effect of friction and blank holder force on the radial stress

Friction between the blank holder and the flange increases the radial stress. Blank holder force can also be considered as a line force of magnitude  $\frac{F_{BHF}}{\pi d_0}$  Per unit length, as can be seen from Fig. 5.

The friction force on the flange, per unit length around the edge, was calculated as follows[29]:

$$\sigma_{r,BHF} = \frac{2\mu F_{BHF}}{\pi d_{1,i} t_0} \quad (19)$$

Where,  $t_0$  is the initial thickness of the sheet,  $F_{BHF}$  is the blank holder force (BHF),  $\mu$  is the friction coefficient and  $d_{1,i}$  is the outer diameter along the punch stroke. Therefore, by applying the blank holder force and considering the effects of sheet anisotropy, the flange's radial stress is calculated according to Eq (20).



**Fig. 5.** Effect of blank holder force on radial stress.

$$\sigma_{r,i} = \sqrt{\frac{2(R+1)}{2R+1}} \sigma_{f1-2,i} \ln\left(\frac{d_{1,i}}{d_i}\right) + \frac{2\mu F_{BHF}}{\pi d_{1,i} t_0} \quad (20)$$

By applying friction on all surfaces in addition to the tension in bending at the die radius, the radial stress Equation is written as follow: [29]

$$\sigma_{r,i} = e^{\left(\frac{\mu\pi}{2}\right)} \left[ \sqrt{\frac{2(R+1)}{2R+1}} \sigma_{f1-2,i} \ln\left(\frac{d_{1,i}}{d_i}\right) + \frac{2\mu F_{BHF}}{\pi d_{1,i} t_0} \right] + \sigma_{f2-3,i} \frac{t_0}{2r_d} \quad (21)$$

### 2.5. Calculation of tearing limit with the energy criterion

As indicated in the introduction, this study's analytical purpose is to calculate the tearing limit with a new criterion based on the strain energy. The first Criterion of cracking was the maximum stress of the material.

$$\sigma_{r,1,crack} \geq c \cdot UTS \quad (22)$$

Previous researchers calculated the tearing limit based on this criterion, Eq (22). Where UTS is the ultimate tensile stress, and c is the cracking factor which should be greater than unity [29]. Since the sheet material is St14 steel in this study, c was considered between 1.05 and 1.55 [29]. In this study, c is considered 1.25, according to tensile tests. This study intends to calculate the tearing limit with the first failure criterion and new criterion based on the strain energy and compare them with simulation and experimental results. The second criteria of failure, which is based on the strain energy, is written as follow:

$$\sigma_{r,2,crack} \cdot \varepsilon_{3,i} \geq c \cdot S_{UTS} \quad (23)$$

So:

$$\sigma_{r,2,crack} \geq \frac{c \cdot S_{UTS}}{\varepsilon_{3,i}} \quad (24)$$

Where  $S_{UTS}$  is the area under the stress-strain curve, and  $\varepsilon_{3,i}$  is the strain at point 3, where tearing happens. According to Eq (23), when the strain energy in each element of the wall reaches critical

energy, tearing would happen in sheet metal. In other words, if it becomes equal to multiple of the area under the stress-strain curve of the uniaxial tensile test, the sheet will be faced tearing. Therefore, if the wall's radial stress ( $\sigma_{r,i}$ ) reaches each of these stresses ( $\sigma_{r,j,crack}$ ), tearing or cracking on the wall will happen. Finally  $F_{BHF,max}$  is obtained using Eq (21). In order to calculate  $F_{BHF,max}$  based on the first and second criterion,  $\sigma_{r,j,crack}$  is, firstly, obtained using either Eq (22), or (24), and  $F_{BHF,max}$  is obtained at different stages of the punch stroke using Eq(25).

$$F_{BHF,max} \leq \frac{\pi d_{1,i} t_0}{2\mu} \left[ \frac{\sigma_{r,j,crack}}{e^{\mu \frac{\pi}{2}}} - \frac{\sigma_{f2-3,i} \frac{t_0}{2r_D}}{e^{\mu \frac{\pi}{2}}} - \sqrt{\frac{2(R+1)}{2R+1}} \sigma_{f1-2,i} \ln \left( \frac{d_{1,i}}{d_i} \right) \right] \quad (25)$$

Therefore, the maximal force is a function of:

$$F_{BHF,max} = f(k, n, UTS, R, t_0, d_0, d_D, r_p, d_{1,i}, h_i, d_{int,i}, \mu) \quad (26)$$

### Finite element method:

In this simulation, a sheet of deformable and 3D element with 1 mm thickness and 200 mm diameter was considered, and other mold parts are simulated in 3D, shell, and rigid instead of the blank, which was considered a 3D and deformable part. For all mold components, the reference points were considered the center of gravity, and each of the volumes was calculated in SOLIDWORKS, and then they were applied in ABAQUS. To extract the sheet's material properties, including modulus of elasticity, stress-strain curve, and anisotropy coefficient, uniaxial tensile tests based on ASTM E8 [31] were applied, as can be seen from Fig. 6(a). In order to obtain anisotropy properties of the sheet, the tensile tests were done on three samples, which had been cut in three different directions, including parallel, perpendicular, and angle of 45 degrees in proportion to the rolling direction. The sheet had a thickness of 1 mm and was tested with a strain rate of  $0.001 \text{ s}^{-1}$ .

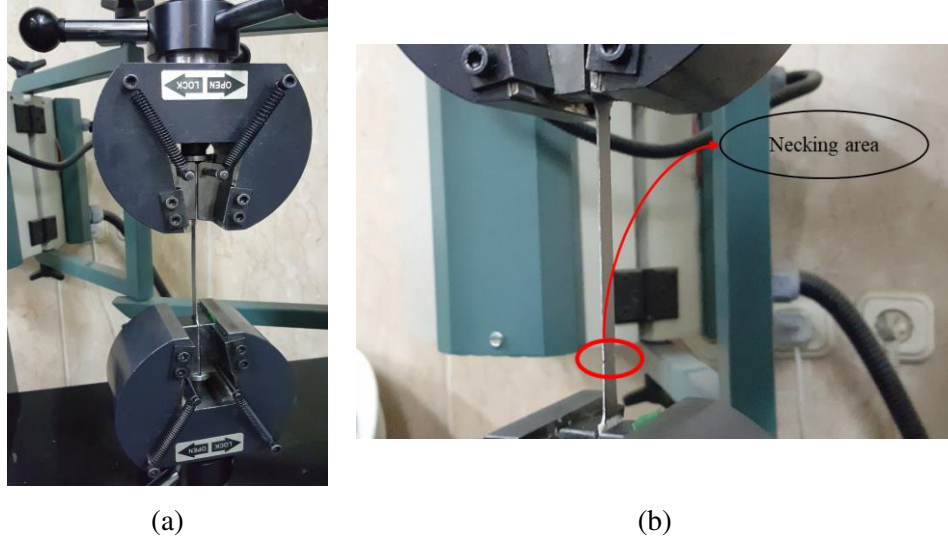


**Fig. 6.** (a) tensile test based on ASTM E8, before necking (b) after necking

Table 1. Mechanical properties of St-14 obtained by uniaxial tensile test

**Table. 1.** sheet metal property ST14

Sample	$E$ (GPa)	$\rho$ ( $\text{kg}/\text{m}^3$ )	$\sigma_y$ (MPa)	$\nu$	UTS. (MPa)
0°	165	7800	155	0.33	410
45°	165	7800	165	0.33	444
90°	165	7800	150	0.33	426

In order to estimate the energy needed for ductile failure, the area under the stress–strain diagram was utilized. Then, the stress–strain data of plastic area was used directly in ABAQUS to simulate sheet’s behavior precisely during metal forming process. To obtain fracture properties of the sheet, and considering that the sheet material is of ductile type. ABAQUS for modeling ductile damage needs three fracture strain triaxial stresses and strain rate parameters along with fracture energy.

$$\sigma = \frac{\sigma_H}{\bar{\sigma}} \quad (27)$$

According to Eq (27), triaxial stress is calculated. For obtaining fracture properties, the test sample should be similar to standard test samples but at the same time should have a groove in the middle with a determined radius. If the model has a circular cross-section, this groove would be trough out, but if the sample has a rectangular cross-section, the groove is made on both sides of the sample. Of course, by considering the radius of the groove, one can calculate the triaxial stress index. If fracture properties are obtained from the standard sample, the related groove radius should

be taken as infinity. Eq (28) is Bridgman modified formula with which the triaxial stress index will work out 0.577 for the standard tensile test sample.

$$\eta = \frac{1}{\sqrt{3}} + \frac{2}{3} \ln\left(1 + \frac{a}{2}\right) \quad (28)$$

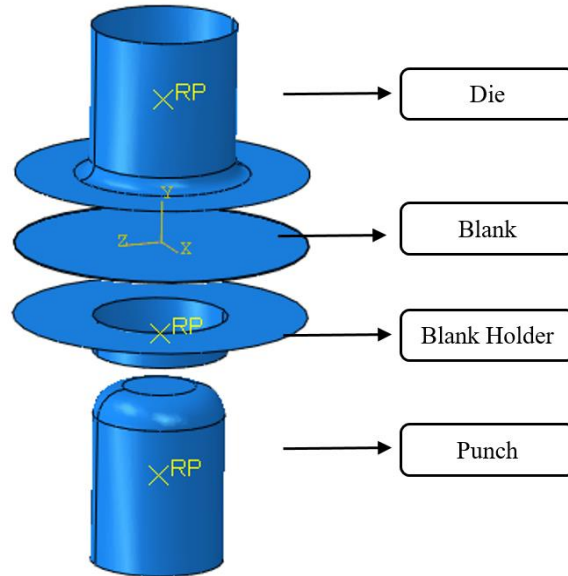


**Fig. 7.** Exploded view from components of the simulated model in ABAQUS

For choosing a suitable element for modeling the sheet, it was referred to the ABAQUS library. With choosing explicit dynamic elements, three-dimensional stress element, C3D8R element was recognized as ideal for studying the process. The continuous shell element is a 3-dimensional element for modeling high and narrow structures with similar sheet behavior. The use of this element is for thin shells, high deformation, and nonlinear behavior. This element is suitable for the thin shell, high deformation, and nonlinear behavior such as the elastoplastic behavior of material like spring back in the deep drawing process. 3D stress element is a solid element for calculating stress-strain in a 3D space, and studying the possibility of sheet tearing during forming is an appropriate option. It should be mentioned this element has sheet properties like fracture strain and fracture energy, which can model sheet tearing but cannot directly show the changes in sheet thickness. The continuum shell element is suitable for studying thickness changes, whereas 3D strain elements can be used to study sheet-tearing possibilities and exchange for each other. It was referred to the ABAQUS library for choosing suitable elements for punch, die, and the other

mold components. Since the components of mold were rigid shell elements, R3D4, was used. This element cannot describe properties for stress-strain calculation because it is used for the rigid surface without strain. It can only calculate and report force, speed, and torch.

### **3. Experiment:**

The experimental cup is an axial symmetrical cylinder with about 60 mm depth, while its initial and final diameters are 200 and 100 mm, respectively. Punch and die materials were chosen from VCN200 steel to avoid heat treatment and provide a good abrasion resistance against tensile strength tests. The internal diameter was taken 2 mm larger than a punch to avoid friction on the die surface. More looseness would cause the blank after forming would come out of the die easily without deformation. Considering that forming height is variable, the height of the die is taken 105 mm. The blank holder was a ring with a 92 mm internal diameter whose external diameter was equal to the die's outer diameter. The blank holder's thickness was chosen 25 mm to have an appropriate resistance against the blank holder force transfer and exertion uniform force to the sheet. Both surfaces of the holder were polished with magnetic grinding to have uniform force transfer on both sides. The punch was designed based on the drawn depth and external diameter of the blank. The material for punch was also VCN200, and the contact surface with sheet and radius of punch angles were the same as the die burnished in three stages. Two rams with st52 material were designed suitable with a hydraulic press and die dimensions. Two standard guideposts for the alignment of mold components were used. In the lower ram, four holes were considered for the passage of press air pin bars. To assembly, the guideposts of mold are fastened to the lower ram with pin and screw, and then the punch is fastened to the middle of the lower ram with pin and screw. The upper ram is also located on guideposts, and after alignment, the holder is placed around the punch, and the die is placed on top of that. Then with the use of standard holders, looseness between punch and die was adjusted. With the use of pins and screws, the die was assembled on the upper ram. Different parts of the manufactured mold are shown in Fig. 8.



(a)



(b)

**Fig.8.** Different parts of the deep drawing mold (a) punch, blank holder, and guidepost (b) Die. It is also crucial to note that parameters, including  $d_0$ ,  $d_D$ ,  $r_p$ ,  $r_D$ ,  $t_0$ , UTS, R, yield stress, are needed to calculate tearing limit; these parameters related to the dimension of mold's elements and sheet properties are listed in table.2.

**Table. 2.** Die's elements dimensions

Definition	Symbol	Unit	Value
Initial sheet diameter	$d_0$	(mm)	200
Die diameter	$d_D$	(mm)	100
Punch radius	$r_p$	(mm)	20
Die radius	$r_D$	(mm)	10
initial sheet thickness	$t_0$	(mm)	1
Ultimate tensile stress	UTS	(MPa)	410
Anisotropy coefficient	R	-	1.03
The area under the stress-strain plot	$S_{UTS}$	(MPa)	151.67
Punch velocity	V	( $mm/s$ )	66
Cracking factor	c	-	1.25

#### 4. Results and discussions

As noted in previous sections, the drawn depth at the tearing moment is calculated as FEM simulation, experiments, and analytical method based on strain energy criterion and previous investigators' criteria, and all the results are compared and verified. This research's main objective is to introduce a new method for estimation of tearing limit by analytical approach. As a result of this, it is necessary to compare and verify the FEM results with that of the experiment to ensure

the simulated model's accuracy. After ensuring that the simulated model is correct, analytical results based on strain energy and previous criterion are compared with FEM simulation results, and the accuracy of each criterion is determined in the estimation of the tearing limit.

#### **4.1. Comparing and verifying FEM simulation and experimental results**

In order to compare and verify FEM simulation with experimental results, First of all, it is imperative to anticipate the safe area by FEM simulation, and then part of the calculated tearing limit in the FEM simulation is compared with and verified by experimental results. The safe area in the deep drawing process is referred to as the area in which it is free from tearing and wrinkling. The deep drawing process was carried out without lubricant. The friction coefficient was 0.2 for all surfaces, and the die speed was 33 mm/s. A sliding friction test was applied to measure the friction between surfaces in contact with each other. Testing took place by dragging a flat block of known mass across a flat table. Graphs of force, displacement, and time were used to measure both static and kinetic frictions. Defining friction coefficients requires precisely and repeatedly measuring peak forces required to initiate (static) and maintain (kinetic) movement. One of the most critical parameters leading to the occurrence of these defects is the BHF. Therefore, researchers present a region as a safe area in which the maximum and minimum force is calculated at different punch stroke stages. In order to calculate safe area by FEM simulation, all parameters were considered constant during the process, and drawn depth was calculated at the moment of tearing or wrinkling of the sheet with various BHFs. FEM simulation was carried out with friction coefficient of 0.2 and the die speed of 33 mm/s, these two parameters are equal to experimental ones, as they are shown in Fig. 9. It is also important to note that  $1.6t_0$  (sheet thickness) is considered as the wrinkling criteria, meaning that when the distance between blank holder and die reach  $1.5t_0$  wrinkling will happen.

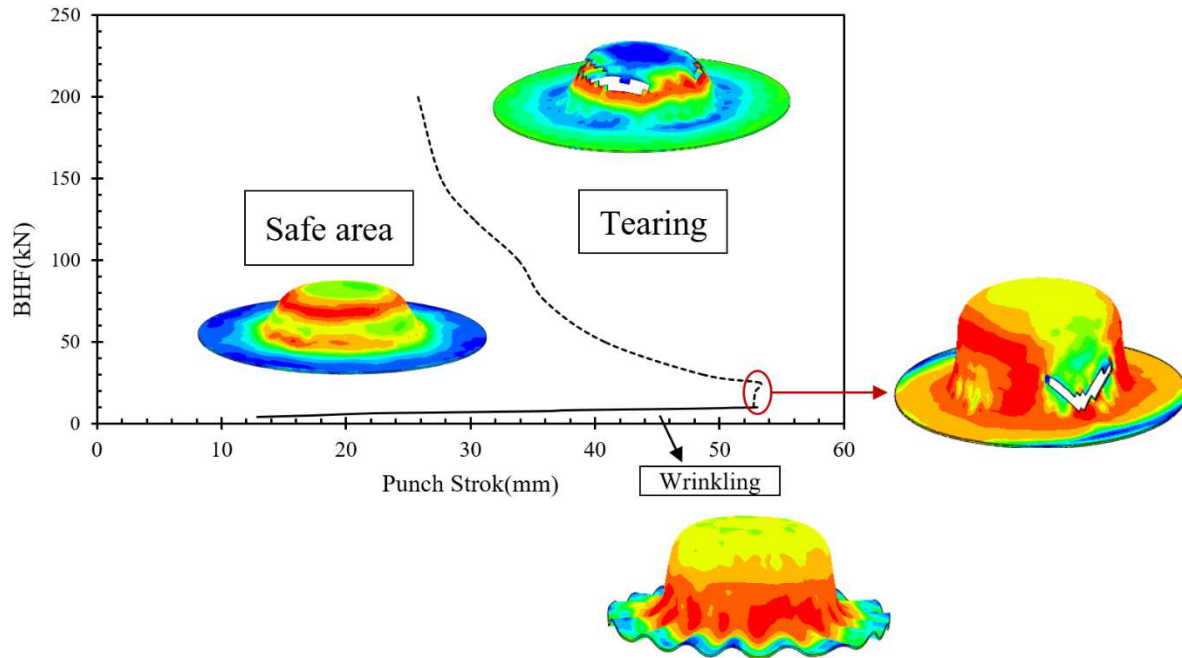


**Fig. 9.** safe area plot with FEM simulation  $\mu = 0.2, v = 33 \frac{mm}{s}$

After simulation and doing experiments with these parameters, it was determined that when the force is greater than 200kN, the sheet cannot move on the blank holder, so drawn depth will not be changed, albeit BHF increasing. Therefore, the forces of over 200kN are not considered in Fig. 9. After simulation and evaluating its results, the safe area is divided into three independent parts, based on the amount of the BHF, and the characteristics of these areas are examined individually.

First area: when BHF was between 25 and 200 KN. In this area, in case of BHF decreasing, the drawn depth will increase, and tearing also happened in the upper region of the cup's wall. The location of the tearing in the first area is shown in Fig. 9.

Second area: when the BHF is between 10 to 25kN, the drawn depth is more than other areas. In this area, drawn depth deviations are much lower than that of the first area. Drawn depth in this area does not have a specific pattern along with changes of BHF (in this area, changes of drawn depth are not uniform).

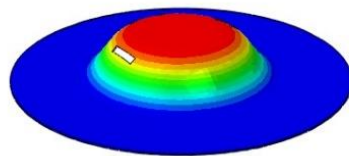
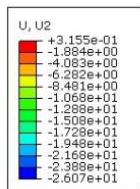
In the second area tearing of the sheet happens in the lower wall of the cup and close to the flange. The location of the tearing in the second area is shown in Fig. 9.

Third area; When the BHF is less than 10kN, the sheet will be wrinkle. Different criteria are used in determining the moment of wrinkling, in most of which, when the distance between the die and blank holder reaches a coefficient of sheet thickness, wrinkling will happen. This coefficient can vary from 1.25 to 2, depending on the sheet's condition and thickness [30]. In this study, the coefficient of wrinkling is considered 1.6. Fig. 9 shows wrinkling in the flange area.

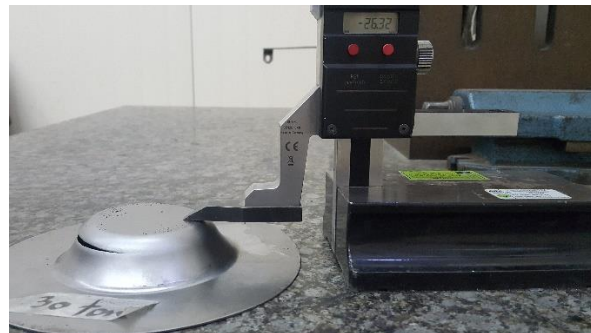
After reviewing these areas' specifications, knowing that drawn depth variations have no specific pattern in the second area, sheet behavior cannot be estimated in this area by plasticity relationships. The experimental and analytical study, accordingly, was conducted merely in the first area. As the determination of drawn depth at the moment of tearing is so difficult in experimental tests and needs a lot of try and error, drawn depth was calculated by five BHF at the moment of tearing, the results of which are shown in Table.3 and Fig. 10 and 11. Considering process parameters when the BHF increases more than 200kN, the BHF is so much that the sheet can hardly move over the blank holder. As simulation and experimental results show, drawn depth at the moment of tearing with a constant BHF of 300 and 250kN are almost equal.

**Table. 3.** Comparison and verification FEM simulation results and experimental results.

Num	EXP, $h_i$ (mm)	FEM, $h_i$ (mm)	BHF (N)
1	39.41	40.79	30000
2	32.36	33.98	100000
3	28.12	27.62	150000
4	26.39	26.03	250000
5	26.72	26.32	300000



(a)



(b)

**Fig .10.**Comparison of the drawn depth at the moment of tearing with the 294kN BHF,  $\mu = 0.2$ ,  $\nu = 33 \frac{mm}{s}$ , (a) drawn depth in the experimental sample: 26.32mm, (b) drawn depth in the FEM simulation sample: 26.38mm

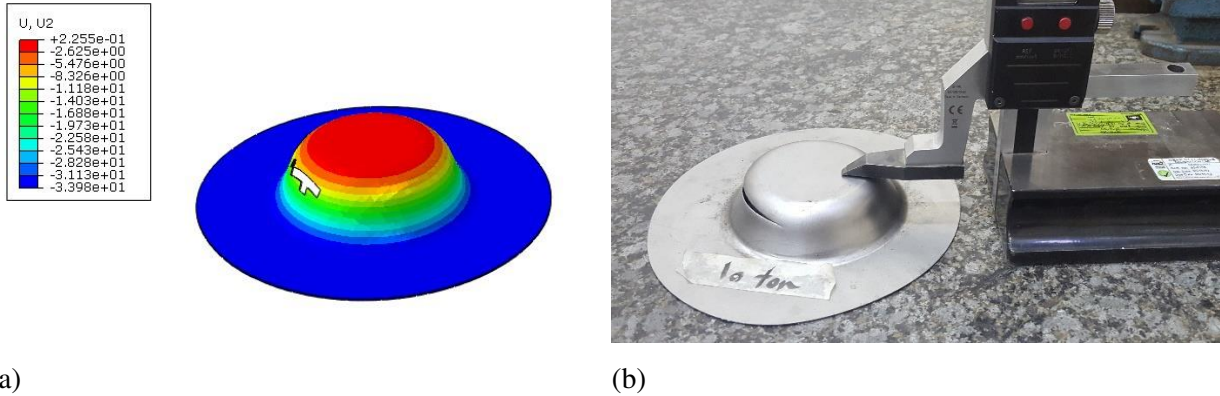


**Fig .11.**Comparison of the drawn depth at the moment of tearing with the 98kN BHF,  $\mu = 0.2$ ,  $\nu = 33 \frac{mm}{s}$ , (a) drawn depth in the experimental sample: 32.36mm, (b) drawn depth in the FEM simulation sample: 34.2mm

#### 4.2.Comparison of analytical and FEM simulation results

This section aims to calculate the tearing limit with the first and second approaches in an analytical method using plasticity relations and compare them with FEM and experimental ones. The tearing limit was calculated by FEM simulation, first criterion Eq (22), and the second criterion Eq (24), separately and compared with each other. The method for calculation of the effective parameters on the tearing limit is that the safe area, at first, is calculated using FEM simulation. After obtaining safe area calculated by FEM and determination of variation range of punch stroke, different values for  $h_i$  in each stage will be specified according to FEM results. With having parameters  $d_{1,i}$ ,  $d_{int,i}$ ,  $\epsilon_{1,i}$ ,  $\epsilon_{2,i}$ ,  $\sigma_{f,1-2,i}$  and  $\sigma_{f,2-3,i}$  respectively, maximum BHF is calculated along punch stroke with the use of Eq (24). Parameters, including  $d_0$ ,  $d_D$ ,  $r_p$ ,  $r_D$ ,  $t_0$ , UTS, R, yield stress, are needed to calculate mentioned items; these parameters related to mold's elements dimensions are listed in table.2.

With the Eq (22), (24), and (25) and having parameters given in Tables 2 and 4, the maximum BHF in each stage of punch stroke is calculated with two strain energy and maximum stress of material criteria, and they are compared with FEM results according to Table 5. It is important to note that in the FEM simulation, BHF is input, and finally,  $h_i$  (drawn depth at the tearing moment) is measured by ABAQUS after finishing the simulation as the output. By contrast, in analytical calculations (the first and second approach),  $h_i$  measured by ABAQUS is considered as the input, and  $BHF_{i,max}$  is eventually calculated by Eq (25) as the output. This process is shown in Fig. 1 in a more detail.

**Table 4.** Analytic calculation of strain and mean flow stress in flange at 3 different points.

$h_i$ (mm)	$d_{1,i}$ (mm)	$d_{int,i}$ (mm)	$\epsilon_{1,i}$	$\epsilon_{2,i}$	$\epsilon_{3,i}$	$\sigma_{f,1-2,i}$ (Mpa)	$\sigma_{f,2-3,i}$ (Mpa)
25	185.3	133.2	0.11	0.27	0.33	306.74	345.48
27	178.4	142.3	0.13	0.29	0.35	331.28	373.76
30	175.3	146.1	0.15	0.32	0.38	340.99	384.38
32	173.2	148.5	0.16	0.34	0.39	347.27	391.06
35	170.1	152.1	0.18	0.37	0.42	356.43	400.54
38	166.9	155.6	0.20	0.4	0.45	409.45	365.36
40	164.7	157.9	0.22	0.41	0.47	371.19	415.10

With the usage of these parameters given in Table. 4. In order to calculate  $F_{BHF,max}$  based on the first and second criterion,  $\sigma_{r,j,crack}$  is, firstly, obtained using either Eq (22), or (24), and  $F_{BHF,max}$  is obtained at different stages of punch stroke according to Eq(25).

**Table 5.** Analytical results for BHF, max;  $\mu = 0.2$

$BHF_{FEM}$ (N)	$BHF_{2,max}$ (N)	$\sigma_{crack,2,i}$ (Mpa)	$BHF_{1,max}$ (N)	$\sigma_{crack,1,i}$ (Mpa)	$h_i$ (mm)
200000	209800	575	85772	450	25
150000	167670	540.91	80562	450	27
125000	120810	498.42	74000	450	30
100000	95692	474.61	71238	450	32
70000	64420	444.07	70287	450	35
55000	40098	450	64271	450	38
30000	26698	403	58696	450	40

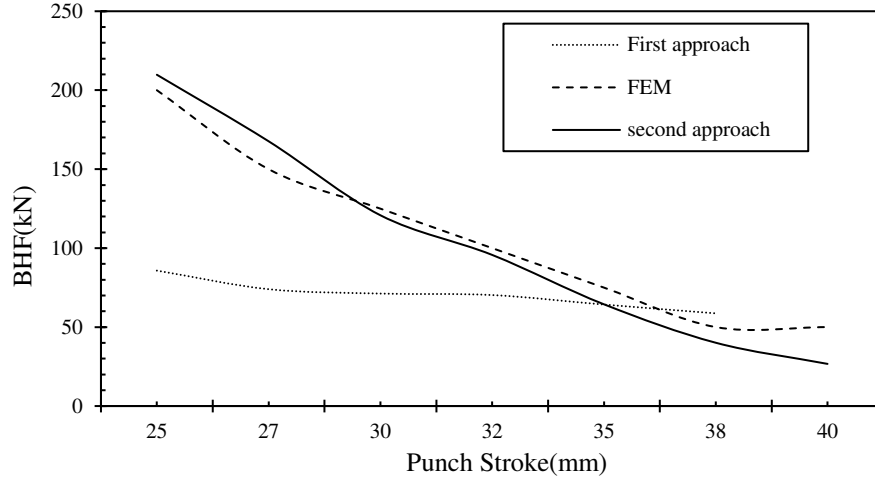


**Fig .12.** Comparison of maximum BHF with energy criteria, UTS criteria, and FEM simulation;  $\mu = 0.2$ .

In Table 5,  $BHF_{1,max}$  is the maximum BHF, which is calculated using the final maximum stress criterion, first criterion,  $BHF_{2,max}$  is the maximum BHF, which is calculated using the strain energy criterion, second criterion, and  $BHF_{FEM}$  is the maximum BHF which was calculated using FEM simulation. As shown in Fig .12. the second approach is strain energy criterion, FEM is FEM simulation, and the first approach is associated with the final maximum stress criterion. As shown in Table 5 and Fig 12, there is considerable consistency between the results related to the strain energy criterion and the second approach. To ensure the correctness of the mathematical model and the new criterion,  $BHF_{max}$  is calculated in two methods of FEM and energy method (second approach) with two other friction coefficients of 0.1 and 0.15, the results of which can be seen from Figs 14 and 15, respectively.

**Table. 6.** Analytic calculation of strain and mean flow stress in flange every punch stroke.  
;  $\mu = 0.1$ .

$h_i$ (mm)	$d_{1,i}$ (mm)	$d_{int,i}$ (mm)	$\epsilon_{1,i}$	$\epsilon_{2,i}$	$\epsilon_{3,i}$	$\sigma_{f,1-2,i}$ (Mpa)	$\sigma_{f,2-3,i}$ (Mpa)	$\sigma_{crack,2,i}$ (Mpa)	$BHF_{2,max}$ (N)
<b>39</b>	165.8	156.7	0.21	0.40	0.46	368.2	412.3	410.3	192109
<b>41</b>	163.4	159.4	0.23	0.42	0.47	374.0	417.8	396.1	161863
<b>43</b>	161.9	161.3	0.24	0.44	0.49	379.8	423.2	383.1	136154
<b>45</b>	159.2	163.5	0.26	0.45	0.51	385.4	428.3	371.4	114512
<b>48</b>	155.7	166.8	0.28	0.47	0.53	393.9	435.8	355.5	88706
<b>51</b>	152.2	170.0	0.31	0.50	0.55	402.2	442.8	341.5	69789
<b>53</b>	149.8	172.8	0.33	0.51	0.57	407.8	447.4	332.9	60772

<b>56</b>	146.2	175.4	0.36	0.53	0.59	416.1	453.9	321.3	51689
<b>58</b>	143.77	177.2	0.38	0.54	0.60	421.7	458.1	314.2	48447

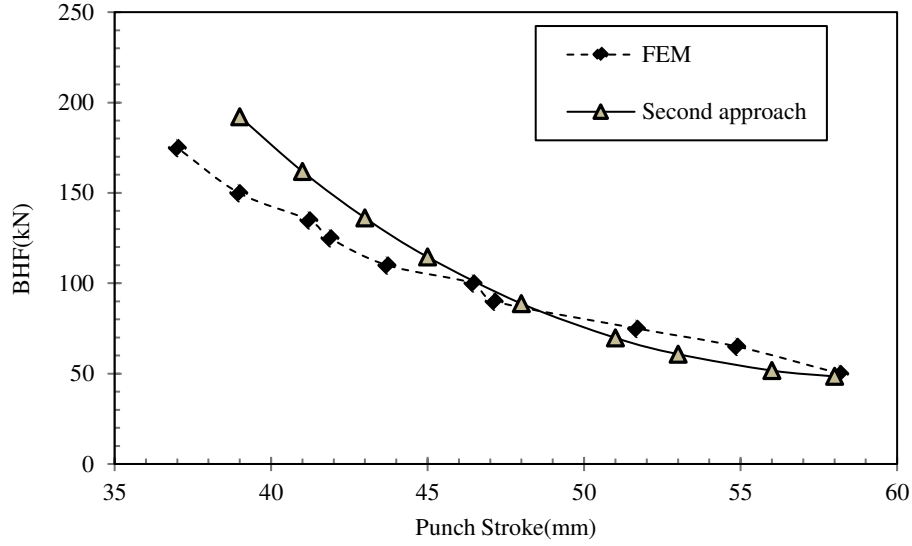


**Fig .14.** Comparison of BHFmax with energy criteria and FEM simulation;  $\mu = 0.1$ .

**Table. 7.** Analytic calculation of strain and mean flow stress in flange every punch stroke.  
;  $\mu = 0.15$ .

$h_i$ (mm)	$d_{1,i}$ (mm)	$d_{int,i}$ (mm)	$\varepsilon_{1,i}$	$\varepsilon_{2,i}$	$\varepsilon_{3,i}$	$\sigma_{f,1-2,i}$ (Mpa)	$\sigma_{f,2-3,i}$ (Mpa)	$\sigma_{crack,2,i}$ (Mpa)	$BHF_{2,max}$ (N)
31	174.3	147.3	0.16	0.34	0.39	344.2	387.7	485.7	194230
33	172.2	149.7	0.17	0.36	0.41	350.4	394.3	463.4	160000
35	170.1	152.1	0.19	0.37	0.43	356.4	400.5	443.7	130693
38	168.0	154.5	0.2	0.39	0.44	362.4	406.5	426.1	100564
39	165.8	156.8	0.22	0.41	0.46	368.3	412.3	410.3	84422
41	163.6	159.1	0.23	0.43	0.48	374.1	417.9	396.1	66463
43	161.4	161.3	0.25	0.44	0.49	379.8	423.2	383.2	51259
45	159.2	163.5	0.26	0.46	0.51	385.5	428.4	371.4	38678
48	155.7	166.8	0.29	0.48	0.53	393.9	435.8	355.5	24021

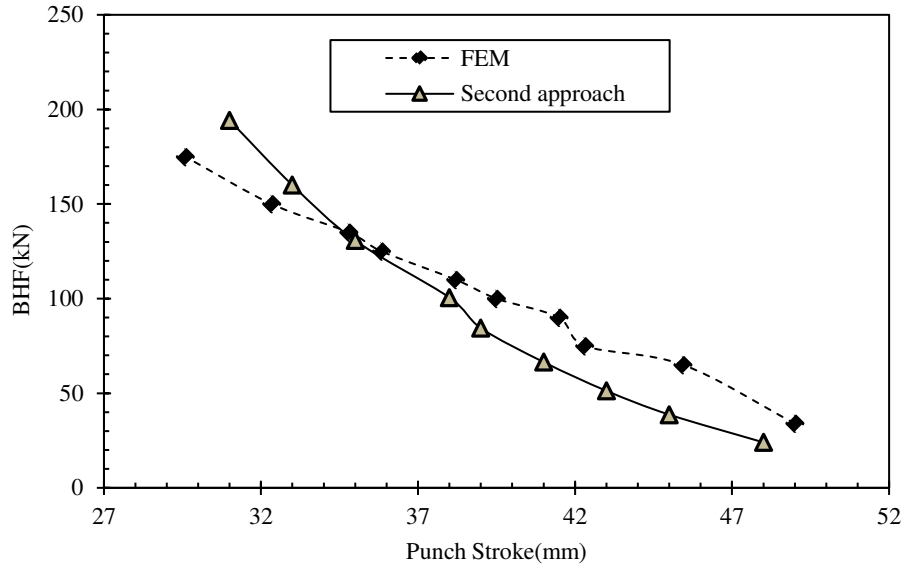


**Fig .15.** Comparison of  $BHF_{max}$  with energy criteria and FEM simulation;  $\mu = 0.15$ .

## 5. Conclusion

A new method based on strain energy was presented for predicting BHF maximum along punch stroke for the first time. Supplementary to this, using dynamic explicit analysis of ABAQUS software, 3D finite element simulation of deep drawing was carried out, in which a new method based on ductile damage was introduced to simulate cracking in sheet metal forming. Additionally, experimental investigations, were carried out to be compared to FEM ones. Firstly, FEM results were verified with experimental ones, demonstrating that the results of these two were considerably close to each other. Then, BHF max was calculated by two criteria, based on strain energy and ultimate tensile stress, and the results of these two approaches were compared with FEM ones. The results related to the strain energy criterion were much closer to the FEM ones in comparison with that of the ultimate tensile stress criterion. Finally, the BHF max was calculated by two new friction coefficients based on the energy strain criterion, and their results were compared to the FEM ones to ensure the new method accuracy. Compared to previous related research, the strain energy criterion would seem to be a better approach to estimate BHF max in the deep drawing process.

**Funding**

There is no funding support for this project.

**Competing Interests**

The authors declare that there are no conflicts of interest/competing interests concerning this paper. In this regard, they have no known competing financial interests or personal relationships that could have appeared to influence the work reported in this paper.

**Availability of data and materials**

All data, material, and codes used in this paper are available.

**Code availability**

All data, material, and codes used in this paper are available.

**Ethical Approval**

This article does not involve human or animal participation or data, therefore ethics approval is not applicable.

**Consent to Participate**

This article does not involve human or animal participation or data, therefore consent to participate is not applicable.

**Consent to Publish**

This article does not involve human or animal participation or data, therefore consent to publication is not applicable.

**Authors Contributions**

The authors' contributions are as following: Mohammad Khaboushani and Ahmad Aminzadeh conceived, planned, and carried out the experiments; Mohammad Khaboushani and Ahmad Aminzadeh contributed to the measurement interpretation, visualization, and analyses of results. Ali Parvizi took the lead in writing the manuscript and Mohammad Khaboushani, Ahmad Aminzadeh and Ali Parvizi contributed actively to writing the manuscript; all authors provided critical feedback and helped shape the research, analysis, and manuscript.

## References

- [1] Tisza M. Development of lightweight steels for automotive applications. *Eng. Steels High Entropy-Alloys*, IntechOpen; 2020.
- [2] Szyndler J, Madej L. Metalforming methods dedicated for the aerospace industry. *Comput Methods Mater Sci* 2015;15:294–310.
- [3] Trzepieciński T. Recent Developments and Trends in Sheet Metal Forming. *Metals (Basel)* 2020;10:779.
- [4] Prakash V, Kumar DR. Performance evaluation of bio-lubricants in strip drawing and deep drawing of an aluminum alloy. *Adv Mater Process Technol* 2020:1–14.
- [5] Dwivedi R, Agnihotri G. Study of deep drawing process parameters. *Mater Today Proc* 2017;4:820–6.
- [6] Tenner J, Andreas K, Radius A, Merklein M. Numerical and experimental investigation of dry deep drawing of aluminum alloys with conventional and coated tool surfaces. *Procedia Eng* 2017;207:2245–50.
- [7] Xiao W-C, Wang B-Y, Kang Y, Ma W-P, Tang X-F. Deep drawing of aluminum alloy 7075 using hot stamping. *Rare Met* 2017;36:485–93.
- [8] Habibi M, Hashemi R, Tafti MF, Assempour A. Experimental investigation of mechanical properties, formability and forming limit diagrams for tailor-welded blanks produced by friction stir welding. *J Manuf Process* 2018;31:310–23.
- [9] Aminzadeh A, Parvizi A, Moradi M. Multi-objective topology optimization of deep drawing dissimilar tailor laser welded blanks; experimental and finite element investigation. *Opt Laser Technol* 2020;125. <https://doi.org/10.1016/j.optlastec.2019.106029>.
- [10] Aminzadeh A, Parvizi A, Safdarian R, Rahmatabadi D. Comparison between laser beam and gas tungsten arc tailored welded blanks via deep drawing. *Proc Inst Mech Eng Part B J Eng Manuf* 2020. <https://doi.org/10.1177/0954405420962391>.
- [11] Padmanabhan KA, Prabu SB, Mulyukov RR, Nazarov A, Imayev RM, Chowdhury SG. *Superplastic Forming, Analyses and Industrial Applications*. Superplasticity, Springer; 2018, p. 359–428.
- [12] Afshin E, Kadkhodayan M. An experimental investigation into the warm deep-drawing process on laminated sheets under various grain sizes. *Mater Des* 2015;87:25–35.

- [13] Reddy ACS, Rajesham S, Reddy PR, Kumar TP, Goverdhan J. An experimental study on effect of process parameters in deep drawing using Taguchi technique. *Int J Eng Sci Technol* 2015;7:21–32.
- [14] Demirci HI, Esner C, Yasar M. Effect of the blank holder force on drawing of aluminum alloy square cup: Theoretical and experimental investigation. *J Mater Process Technol* 2008;206:152–60.
- [15] Choudhari CS, Khasbage SS. Experimental investigation of forming parameters for square cup deep drawing process. *Mater Today Proc* 2020.
- [16] Rubio EM, Camacho AM, Sevilla L, Sebastian MA. Calculation of the forward tension in drawing processes. *J Mater Process Technol* 2005;162:551–7.
- [17] Agrawal A, Reddy NV, Dixit PM. Determination of optimum process parameters for wrinkle free products in deep drawing process. *J Mater Process Technol* 2007;191:51–4.
- [18] Rubio EM. Analytical methods application to the study of tube drawing processes with fixed conical inner plug: Slab and upper bound methods. *J Achiev Mater Manuf Eng* 2006;14:119–30.
- [19] Bamdad AH, Hashemi R. Analytical and numerical investigation of wrinkling limit diagram in deep drawing of two-layer sheets with experimental verification. *Proc Inst Mech Eng Part L J Mater Des Appl* n.d.:1464420720985315.
- [20] Morovvati MR, Mollaei-Dariani B, Asadian-Ardakani MH. A theoretical, numerical, and experimental investigation of plastic wrinkling of circular two-layer sheet metal in the deep drawing. *J Mater Process Technol* 2010;210:1738–47.
- [21] Gharib H, Wifi AS, Younan M, Nassef A. Optimization of the blank holder force in cup drawing. *Optimization* 2006;1:8.
- [22] Aminzadeh A, Karganroudi SS, Barka N. A novel approach of residual stress prediction in ST-14/ST-44 laser welded blanks; mechanical characterization and experimental validation. *Mater Lett* 2021;285:129193.
- [23] Sugiyanto D, Asbanu H, Siahaan FS. The effect of blank holder on the deep drawing process on plates using software based with a Finite Element Method (FEM). *J. Phys. Conf. Ser.*, vol. 1469, 2020, p. 12038.
- [24] Bagherzadeh S, Mirnia MJ, Dariani BM. Numerical and experimental investigations of hydro-mechanical deep drawing process of laminated aluminum/steel sheets. *J Manuf Process* 2015;18:131–40.

- [25] Yoshihara S, Manabe K, Nishimura H. Effect of blank holder force control in deep-drawing process of magnesium alloy sheet. *J Mater Process Technol* 2005;170:579–85.
- [26] Sheng ZQ, Jirathearanat S, Altan T. Adaptive FEM simulation for prediction of variable blank holder force in conical cup drawing. *Int J Mach Tools Manuf* 2004;44:487–94.
- [27] Qin S, Zhang H, Mao Y, Yang L, Li X, Hu Z, et al. Electropermanent magnet blank holder technique in sheet metal deep drawing. *Int J Adv Manuf Technol* 2020;106:5497–507.
- [28] Lange, K. *Handbook of Metal Forming*. USA: Mc-Graw Hill, USA;1985. p. 20.1-20.66.
- [29] Candra, Susila, et al. "Analytical study and FEM simulation of the maximum varying blank holder force to prevent cracking on cylindrical cup deep drawing." *Procedia Cirp* 26 (2015): 548-553.
- [30] Kitayama, S., et al. (2010). "A closed-loop type algorithm for determination of variable blank holder force trajectory and its application to square cup deep drawing." *The International Journal of Advanced Manufacturing Technology* **51**(5-8): 507-517.
- [31] ASTM, E8–99. "Standard test methods for tension testing of metallic materials." Annual book of ASTM standards. ASTM (2001).